

https://doi.org/10.1070/QEL17485

Microstructured optical fibres with a wide single-mode range

A.N. Denisov, S.L. Semjonov

Abstract. **We have proposed a new design of microstructured optical fibres (MOFs), containing three rings of identical circular holes around a core, with different separations between the rings. The properties of the MOFs have been analysed numerically using the finite element method (FEM), and the leakage loss in the spectral range 0.40–2.65 μm has been calculated for the fundamental and higher order modes at various parameters of the MOFs. We have demonstrated the presence of several local maxima in the spectral dependences of the leakage loss for higher order modes and examined the physical mechanism responsible for the formation of the maxima and the variation of their position with MOF parameters. It has been shown that the proposed MOF design allows for single-mode operation in the range 0.77–2.3 μm.**

Keywords: *microstructured optical fibres, single-mode fibres, finite element method.*

1. Introduction

Microstructured optical fibres (MOFs) made of pure silica glass and consisting of a core a few microns in diameter and a cladding containing relatively large holes offer high nonlinearity and have great potential for a variety of scientific and technological applications, such as supercontinuum generation and four-wave mixing [1–4]. Many applications require good beam quality as well, which can be ensured by single-mode fibre. In MOFs with a classic hexagonal configuration of holes, one can in principle obtain endlessly single-mode operation (or so-called endlessly single-mode fibres) [5], but this requires that the hole diameter d and the centre-to-centre distance between the holes Λ meet the relation $d/\Lambda < 0.406$ [6]. In addition, to ensure a low level of leakage losses the number of rings of holes should be sufficiently large, which makes them more difficult to fabricate.

The feasibility of achieving single-mode operation in MOFs with a small number of holes was examined in a number of studies [7–13] concerned with so-called leakage channel fibres (LCFs). However, major attention has been paid to MOFs with a large core diameter (above 20 μm) and one or two rings of holes. The configurations examined so far demonstrate the possibility of adjusting d and Λ so as to ensure a low level of leakage losses (under 0.1 dB m^{-1}) for the fundamental mode and, at the same time, a high level of leakage losses (above 1.0 dB m^{-1}) for higher order modes, which ensures single-mode operation of the MOF [8]. Note that single-mode operation in the MOFs considered in the studies in question is only possible in a narrow spectral range, which is quite sufficient for a number of applications, including transmission of high-power laser light of constant wavelength, and for use in fibre amplifiers and lasers. At the same time, some applications, such as supercontinuum generation, require a much wider single-mode range.

Fini [9] theoretically considered an MOF having a doped core and two rings of identical circular holes arranged in hexagonal order (so-called hole-assisted fibre). The holes in one ring were distance Λ_1 apart, and those in the other ring were distance Λ_2 apart. Suppression of higher order core modes was attributed by Fini [9] to their resonance interaction with very leaky cladding modes because they had identical effective indices.

2. Geometric structure of new MOFs

In this work, we propose a new geometric structure of MOFs, which includes three rings of identical circular holes around its core, the third ring being incomplete and consisting of only 12 holes, so that the total number of holes is 30. We designate this configuration as MOF-30, where the number corresponds to the total number of holes (Fig. 1). The core of the MOF-30, of diameter D_{core}, is shown in Fig. 1 by a dashed line. The holes of the first (innermost) ring are distance Λ_1 apart. The hole diameter d is given by

$$d = \frac{D_{\text{core}}\, R}{(2 - R)}. \tag{1}$$

where $d/\Lambda_1 \equiv R$ is a variable ratio.

The holes of the second ring are distance $\Lambda_2 \geqslant \Lambda_1$ from the nearest hole(s) of the first ring, and the holes of the third ring are distance $\Lambda_3 \geqslant \Lambda_1$ from the nearest holes of the second ring. The spacing Z_{12} between the holes of the first and second rings is

$$Z_{12} = \Lambda_2 - d. \tag{2}$$

This algorithm for constructing the structure of MOF-30 ensures constant Z_{12} for all pairs of holes in the first and second rings but causes the shape of the second ring to differ slightly from a hexagonal one. For convenience, the region between the holes of the first and second rings will hereafter be referred to as the annular space.

A.N. Denisov, S.L. Semjonov Dianov Fiber Optics Research Center, Prokhorov General Physics Institute, Russian Academy of Sciences, ul. Vavilova 38, 119333 Moscow, Russia; e-mail: denisov@fo.gpi.ru

Received 18 November 2020
Kvantovaya Elektronika **51** (3) 240–247 (2021)
Translated by O.M.Tsarev

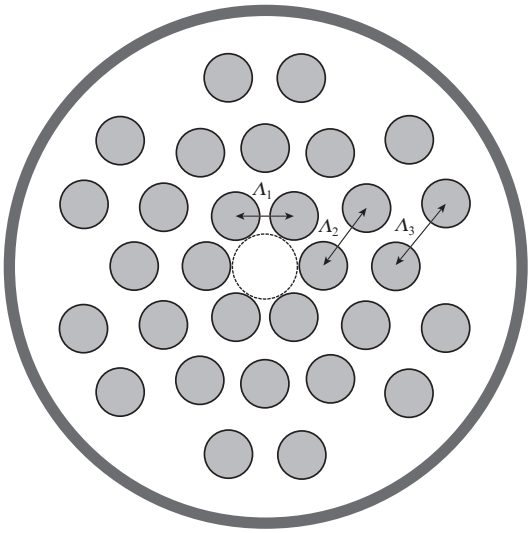

Figure 1. Structure of MOF-30 at $d/\Lambda_1 = 0.82$, $d/\Lambda_2 = 0.66$, and $d/\Lambda_3 = 0.59$.

Since the third ring of holes is incomplete, there is no second annular space, but the presence of an incomplete ring may extend the single-mode range. For example, as shown by Wong et al. [8], an MOF having two rings of holes allows one to obtain a somewhat wider single-mode range than does an MOF having one ring of holes. Besides, this offers additional possibilities for optimising the structure of MOFs by varying their parameters d/Λ_1, d/Λ_2, and d/Λ_3.

3. Calculation results

Characteristics of the MOF were calculated numerically using the finite element method (FEM) with a cylindrical perfectly matched layer (PML), which is represented by a dark grey ring in Fig. 1. It is worth noting that the FEM allows effective modal complex refractive indices and mode field distributions to be calculated for MOFs with an arbitrary shape and arrangement of air holes, which ensures high accuracy of results [14]. Silica glass was taken as the MOF material, and its refractive index was determined using the Sellmeier equation [15]. The leakage loss α (in dB m^{-1}) was determined by the parameter obtained in calculations of the imaginary part of the effective refractive index, k_{eff}, using the relation [16]

$$\alpha = \frac{20}{\ln(10)} \frac{2\pi}{\lambda} k_{\text{eff}}. \qquad (3)$$

Calculations were performed for MOF-30 with a core diameter $D_{\text{core}} = 3.27$ μm. At each of the d/Λ_1 values chosen, we determined the parameters d/Λ_2 and d/Λ_3 (taking $d/\Lambda_3 = d/\Lambda_2$ in the first step) that ensured a fundamental mode leakage loss of 0.1 dB m^{-1} ± 0.1% at a wavelength of 2.3 μm. This dictated the choice of the long-wavelength edge of the single-mode range: $\lambda_{\text{LW}} = 2.3$ μm. Next, we calculated the leakage loss for two fundamental modes differing in polarisation (arbitrarily designated as 1 and 2) and four higher order ring modes (designated as 3 to 6 in the order of decreasing real part of their effective index, n_{eff}) and found the short-wavelength edge of the single-mode range, λ_{SW} (the leakage loss for higher order modes above 1.0 dB m^{-1}).

If necessary for solving any particular problem, one should choose the required edge λ_{LW} and the required level of fundamental mode losses at this wavelength, as well as the

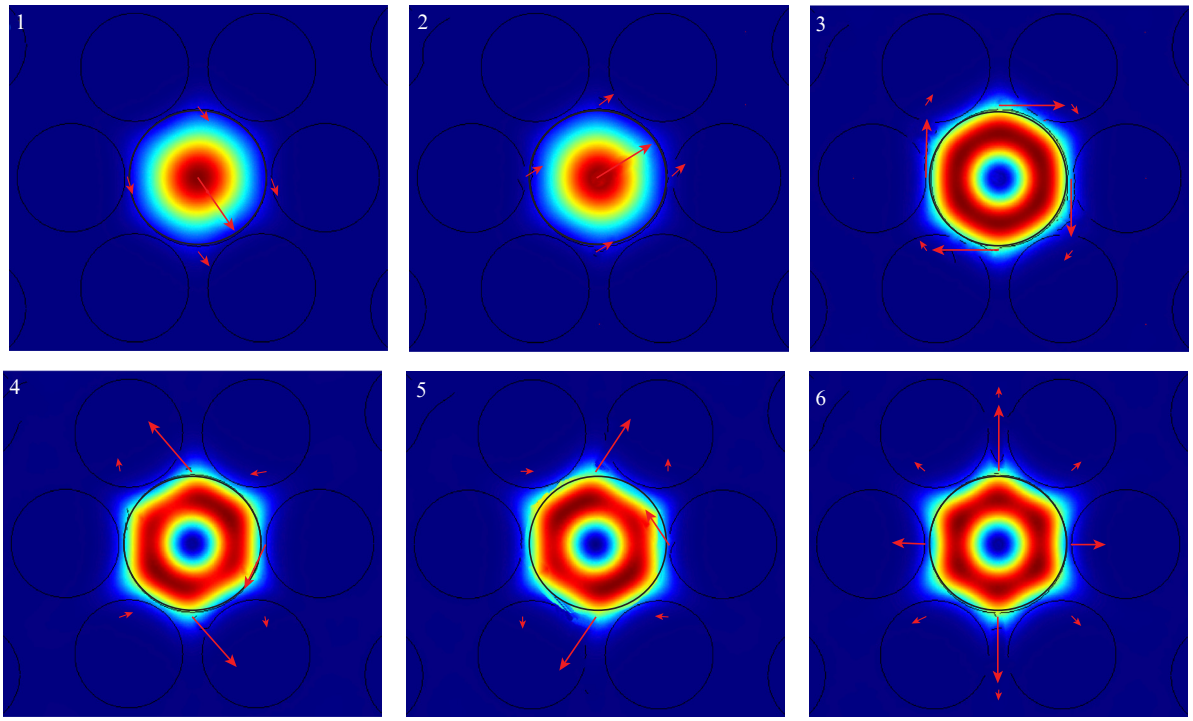

Figure 2. (Colour online) Spatial intensity distributions for the (1, 2) fundamental and (3–6) higher order modes of MOF-30 at $d/\Lambda_1 = 0.85$ and a wavelength of 1.5 μm.

minimum level of losses for higher order modes, and perform the corresponding calculations.

Figure 2 shows spatial intensity distributions for the fundamental (1,2) and higher order (3–6) modes of MOF-30 at $d/\Lambda_1 = 0.85$ and a wavelength $\lambda = 1.5$ μm. These are modes 1 and 2 (HE_{11} species), differing only in polarisation; mode 3 (TE_{01}); modes 4 and 5 (HE_{21}), differing in the direction of the electric field vector and mirror symmetric to each other; and mode 6 (TM_{01}) [17].

Figure 3 shows examples of spectral dependences of the leakage loss for the fundamental mode 1 and three higher order modes at different d/Λ_1 values. The leakage loss for the fundamental mode 1 is essentially identical to that for the fundamental mode 2, so they are represented by the same curves. The losses for modes 4 and 5 are also essentially identical (and are also represented by the same curves). In addition, Fig. 3 shows loss levels of 0.1 and 1.0 dB m^{-1}, which allows one to find the λ_{LW} and λ_{SW} edges [8].

As seen in Figs 3b–3e, the spectral dependences of the leakage loss for higher order modes have a complex character, with local maxima at different wavelengths for different higher order modes. The curves for modes 3 and 6 each have

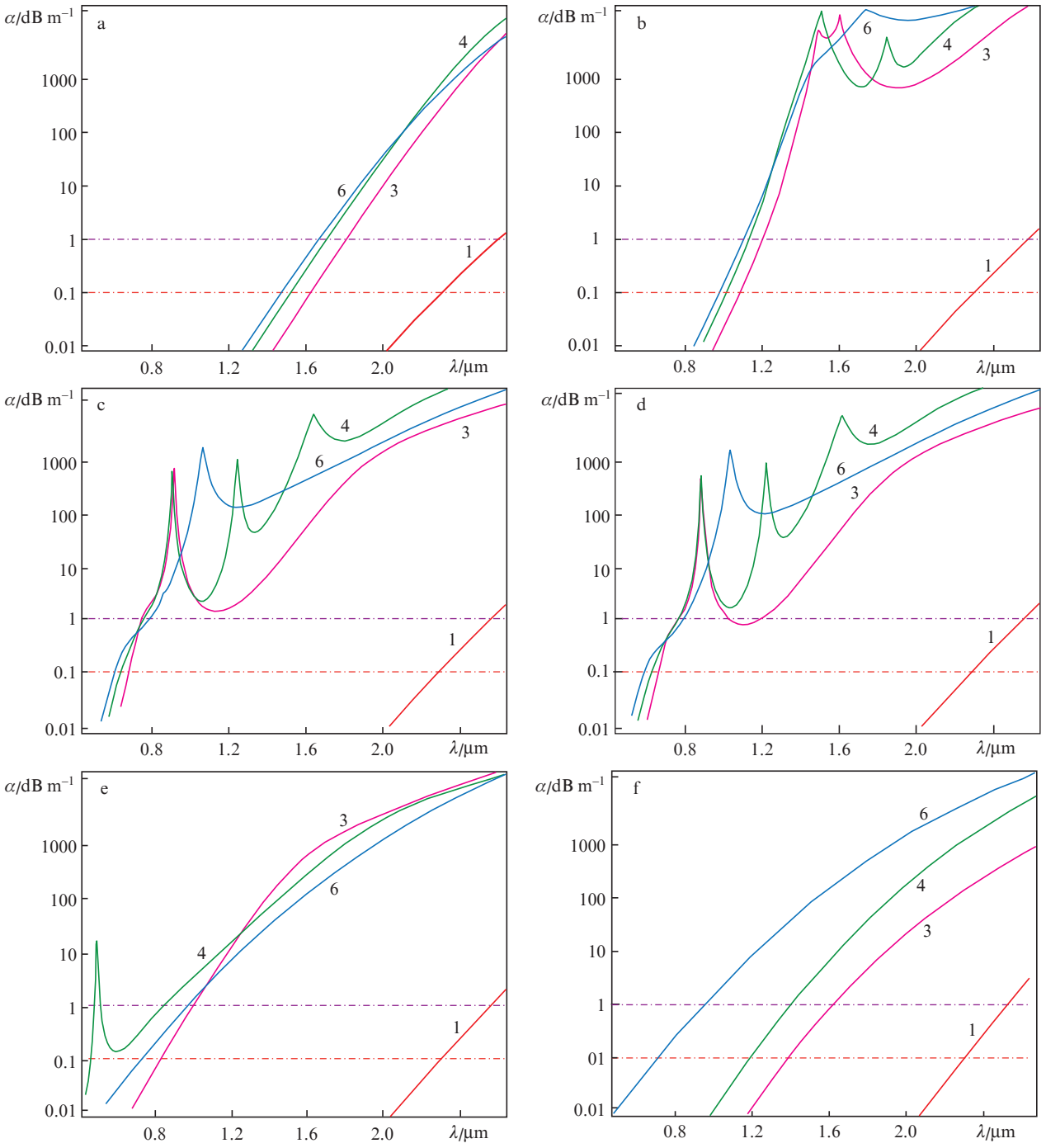

Figure 3. (Colour online) Spectral dependences of the leakage loss in MOF-30 for the (1) fundamental and (3–6) higher order modes at d/Λ_1 = (a) 0.743, (b) 0.800, (c) 0.820, (d) 0.821, (e) 0.850, and (f) 0.900.

one maximum (the corresponding wavelengths are designated as λ_{m3} and λ_{m6}), and mode 4 (along with mode 5) has three peaks, designated as λ_{m4s}, λ_{m4m}, and λ_{m4l}, in the order of increasing wavelength. Figure 4 shows the positions of these peaks as functions of the width of the annular space, Z_{12}. As follows from Fig. 4, Z_{12} ranges from 1.00 to 1.25 μm and, with increasing Z_{12}, changes in peak positions decrease almost linearly.

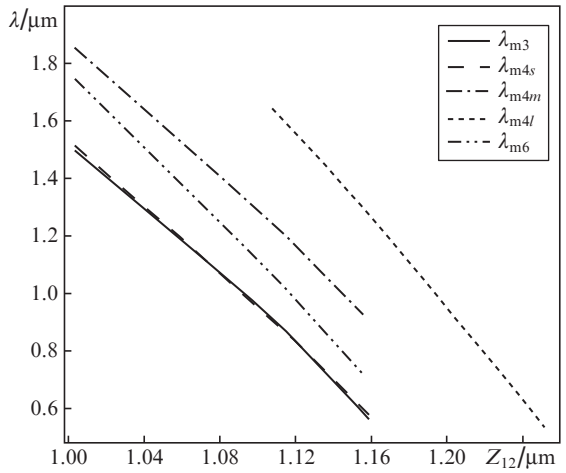

Figure 4. Positions λ_{mi} (i = 3, 4, 6) of the local maxima in leakage loss as functions of the width of the annular space, Z_{12}, for the corresponding higher order modes.

It should be emphasised that all the local maxima in the leakage loss for the higher order modes have a rather high 'background' level, which considerably exceeds 1 dB m^{-1} in most of the spectral range under consideration (Figs 3b–3e). Thus, the local maxima have essentially no effect on the short-wavelength edge of the single-mode range, λ_{SM}, which is determined mainly by the background level. A small exception is observed at $d/\Lambda_1 \approx 0.82$, as suggested by comparison of Figs 3c and 3d. In particular, with decreasing wavelength the background level of losses for mode 3 at $d/\Lambda_1 = 0.821$ (Fig. 3d) becomes less than 1 dB m^{-1} at $\lambda = 1.175$ μm. After that, however, owing to a local maximum the leakage loss again exceeds 1 dB m^{-1} (for $\lambda < 1.032$ μm). On the whole, at d/Λ_1 from 0.8206 to 0.8260, the single-mode range can be divided into two portions, with a small gap between them where the leakage loss for mode 3 is slightly below 1 dB m^{-1}.

Figure 5a shows the width of the single-mode range as a function of d/Λ_1 for MOF-30 (region 1). Region 2 ($\lambda > \lambda_{LW}$) corresponds to the parameters at which the fundamental mode leakage loss exceeds 0.1 dB m^{-1}, and region 3, to a leakage loss for one or a few higher order modes under 1.0 dB m^{-1}. The feature mentioned above shows up here as a rather narrow local minimum with $\lambda_{SW} = 0.77$ μm at $d/\Lambda_1 = 0.82$.

Beyond the local minimum, λ_{SW} is a rather smooth function of d/Λ_1, with a minimum $\lambda_{SW} = 1.01$ at $d/\Lambda_1 = 0.85$ (Fig. 5a). In effect, this behaviour reflects the influence of the d/Λ_1 ratio on the short-wavelength edge of the 'background' level of leakage losses and indicates that there is an optimal value of d/Λ_1 at which the single-mode range has the maximum width.

Figure 5b shows the width of the annular space, Z_{12}, as a function of the d/Λ_1 ratio at which the fundamental mode

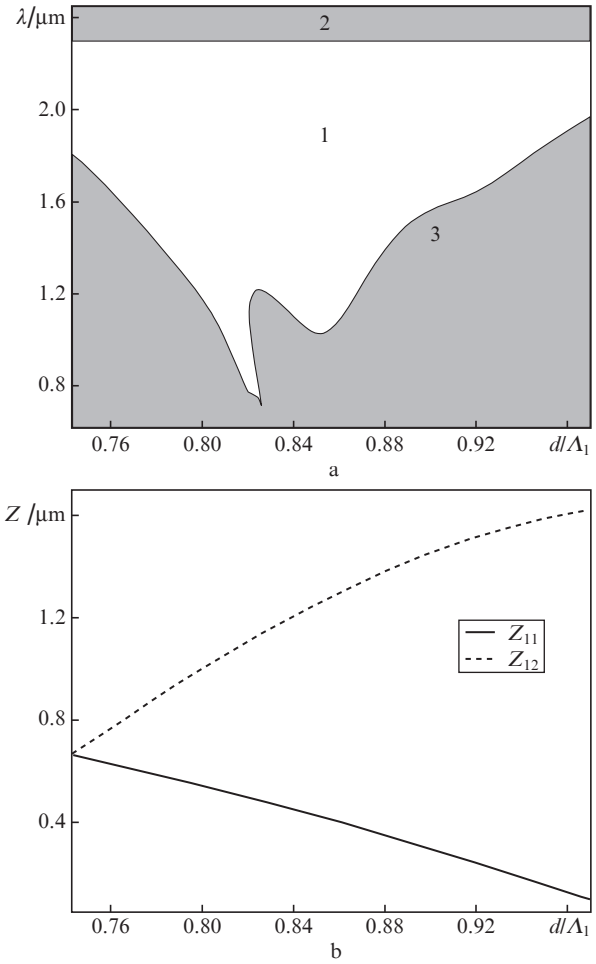

Figure 5. (a) Single-mode range of MOF-30 (region 1) and (b) hole spacings Z_{11} and Z_{12} as functions of d/Λ_1.

leakage loss at a wavelength of 2.3 μm is 0.1 dB m^{-1}. Also shown in Fig. 5b is the spacing between the holes of the first ring, Z_{11}, as a function of d/Λ_1. Using (1), we can obtain the relation

$$Z_{11} = \frac{D_{core}(1-R)}{(2-R)}. \qquad (4)$$

To $d/\Lambda_1 = d/\Lambda_2 = 0.743$ there corresponds a usual hexagonal configuration, in which $Z_{11} = Z_{12}$ and the single-mode range is relatively narrow: 1.81–2.3 μm.

4. Discussion

To find out the origin of the local maxima in the spectral dependences of the leakage loss for higher order modes, consider in greater detail these dependences, as exemplified by that of mode 3 of MOF-30 at $d/\Lambda_1 = 0.821$. Figure 6 shows spatial intensity distributions for mode 3 at several wavelengths near the local maximum at $\lambda_{m3} = 0.883$ μm.

Note first of all that, near the local maximum, there are two modes related to mode 3, as evidenced by the fact that their spatial intensity distributions in the MOF-30 core are similar to those in Fig. 2c. At the same time, they differ slightly in the real part of the effective index, n_{eff}, so for convenience we arbitrarily designate them as 3a and 3b, in the order of decreasing n_{eff}. Since one priority issue for our pur-

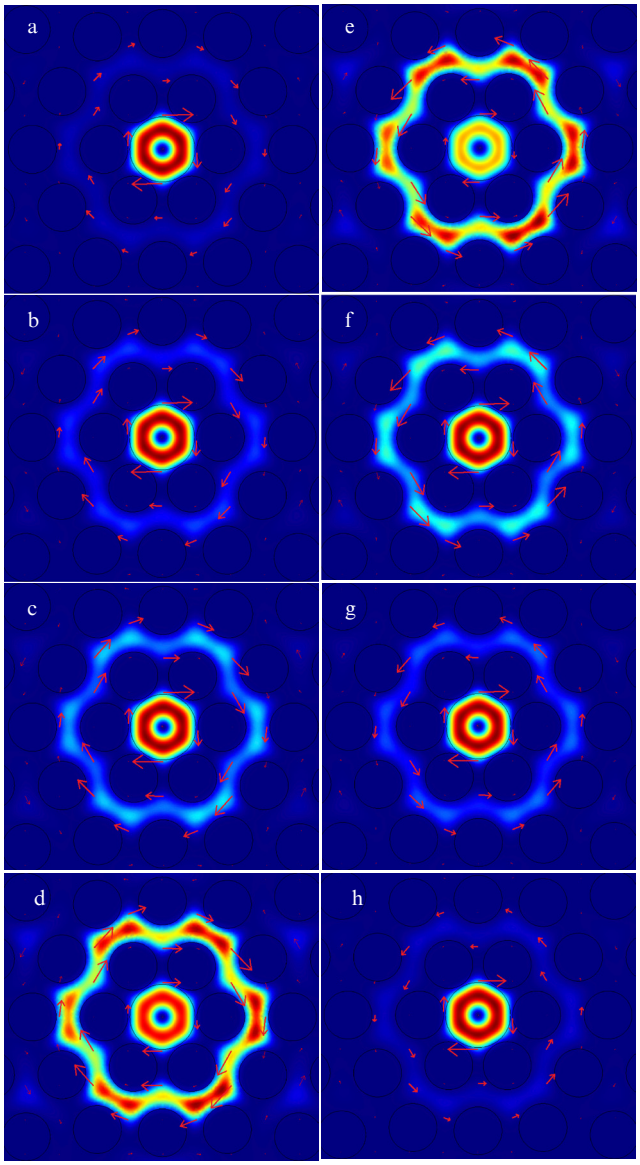

Figure 6. (Colour online) Spatial intensity distributions for modes (a–d) 3a and (e–h) 3b at wavelengths of (a,e) 0.878, (b,f) 0.882, (c,g) 0.884, and (d,h) 0.888 μm.

pose – to find the single-mode range of MOF-30 – is to assess the minimum loss for higher order modes, for the spectral dependences in Fig. 3, of the two modes 3a and 3b we certainly choose the one which has a lower leakage loss at a particular wavelength. Figures 6a–6d show spatial intensity distributions for mode 3a at wavelengths of 0.878, 0.882, 0.884, and 0.888 μm, respectively, and Figs 6e–6h show spatial intensity distributions for mode 3b at the same wavelengths.

As seen in Fig. 6, modes 3a and 3b have additional intensity maxima in the annular space (i.e. in the region of the cladding), and the key distinction of the additional maxima for these modes is related to the orientation of the electric field vector: it is directed clockwise for mode 3a (like the electric field vector of the mode in the MOF-30 core) and counterclockwise for mode 3b. Thus, in the spectral range near the local maximum at $\lambda_{m3} = 0.883$ μm, modes 3a and 3b are localised to a significant degree in the cladding as well. i.e. they are not purely core modes and should be viewed as modes of MOF-30 as a whole.

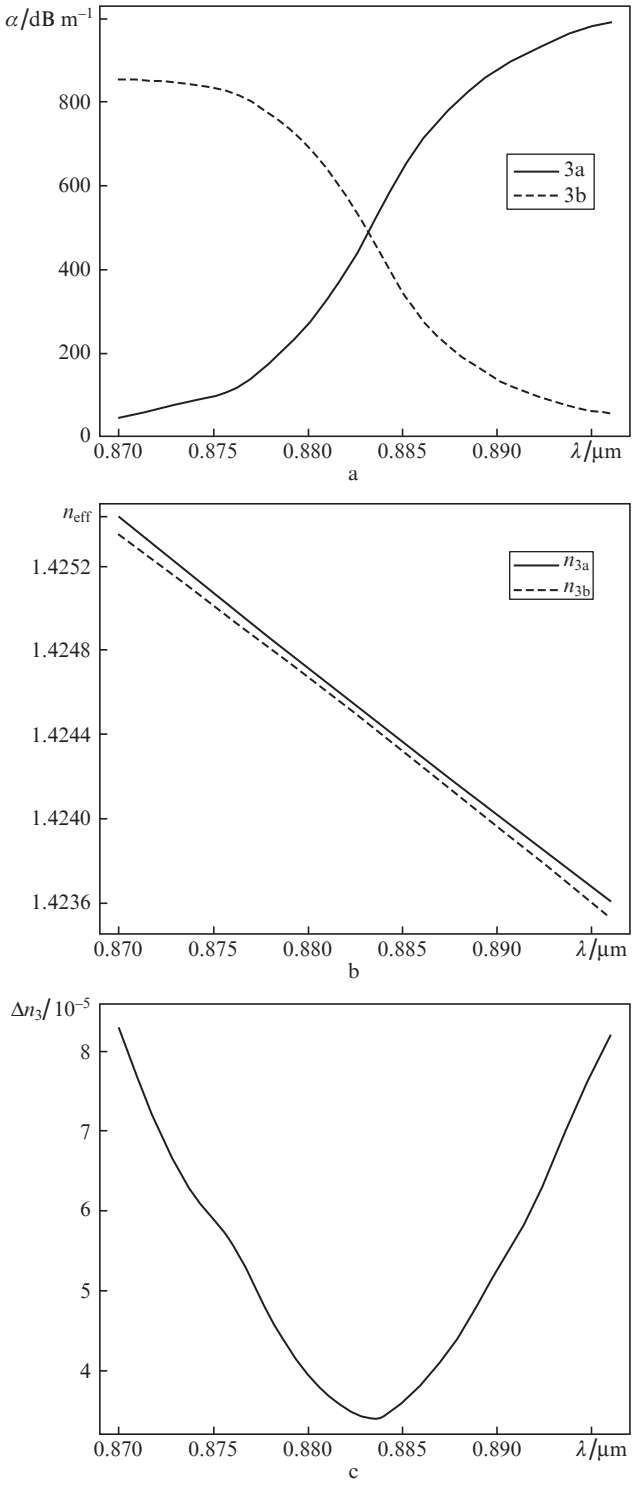

Figure 7. Spectral dependences of (a) the leakage loss, (b) the effective indices n_{3a} and n_{3b}, and (c) the effective index difference $\Delta n_3 = n_{3a} - n_{3b}$ for modes 3a and 3b.

It also follows from Fig. 6 that the additional maxima of modes 3a and 3b in the annular space have different spectral dependences of their intensities. In the case of mode 3a, the intensity of the additional maxima in the range 0.878–0.888 μm rises with increasing λ, which is accompanied by a decrease in the intensity of its main maximum in the MOF-30 core, whereas in the case of mode 3b these intensities vary in the opposite manner. Thus, far away from the local maximum at

λ_{m3}, in the short-wavelength spectral region, to mode 3a there corresponds only the main intensity maximum in the MOF-30 core and to mode 3b correspond only intensity maxima in the annular space, i.e. mode 3b becomes a ring mode of the cladding. In contrast, in the long-wavelength spectral region, far away from λ_{m3}, to mode 3b there corresponds only the main intensity maximum in the MOF-30 core and to mode 3a correspond only intensity maxima in the annular space, i.e. mode 3a becomes a ring mode of the cladding.

Figure 7a shows spectral dependences of leakage loss for modes 3a and 3b in the wavelength range 0.870–0.896 μm. The shape of the curves is quite consistent with the described variation in the intensity of the additional maxima of these modes in the annular space. Increasing λ increases the integrated fraction of the intensity of mode 3a in the annular space, located sufficiently close to the outer boundary of the cladding, which eventually leads to an increase in the leakage loss of mode 3a. In contrast, in the case of mode 3b the leakage loss rises with decreasing λ, and this is also related to the increase in the integrated fraction of its intensity in the annular space. The overall spectral dependence of the leakage loss for mode 3 in this range (Fig. 3d) is the sum of the two lower parts of the curves for modes 3a and 3b in Fig. 7a. Even though the curve with a sharp peak at the wavelength λ_{m3} resembles a resonance dependence, actually there is no loss level resonance and the leakage loss varies rather smoothly but in opposite ways for modes 3a and 3b.

On the other hand, since this variation occurs in a narrow spectral range (about 20 nm), it can be formally described as a quasi-resonance transformation of the higher order core mode 3a into a ring mode of the cladding as the wavelength increases, accompanied by the transformation of the ring cladding mode 3b into a higher order core mode. As shown above (Fig. 4), the quasi-resonance wavelength λ_{m3} depends on the width of the annular space, Z_{12}, and in general on some other parameters of MOF-30, which are taken here to be constant. It is quite likely that λ_{m3} depends on the core diameter D_{core} because the radial intensity distribution of mode 3 in the core depends on its diameter. A more detailed analysis of how parameters of MOF-30 influence λ_{m3} (and the λ_{mi} of other modes) will be the subject of further investigation.

The physical mechanism of the quasi-resonance mode transformation upon variations in wavelength near λ_{m3} is related to the effect of MOF-30 structure parameters (primarily of the width of the annular space, Z_{12}) on the spatial intensity distributions of modes 3a and 3b, which shows up in a narrow spectral range. This causes the relationship between the integrated mode intensities in the core and annular space of the fibre to vary with wavelength. The distinction between the behaviours of modes 3a and 3b seems to result from the above-mentioned distinction between the orientations of the electric field vectors of these modes in the annular space.

Figure 7b shows spectral dependences of the real part of the effective indices n_{3a} and n_{3b} for modes 3a and 3b in the wavelength range 0.870–0.896 μm. It is seen that the data deviate from linearity: obviously, n_{3a} and n_{3b} approach each other near the wavelength λ_{m3}. For better clarity, Fig. 7c shows the spectral dependence of $\Delta n_3 = n_{3a} - n_{3b}$ in this range, which demonstrates that $\Delta n_3 \sim 3.5 \times 10^{-5}$ in the centre of the range and $\Delta n_3 > 8.1 \times 10^{-5}$ at its edges.

This behaviour can be qualitatively explained using the Kramers–Kronig relations, which reflect the principle of causality and, in this particular case, mean that absorption (loss) at some wavelength leads to a non-unity refractive index, and

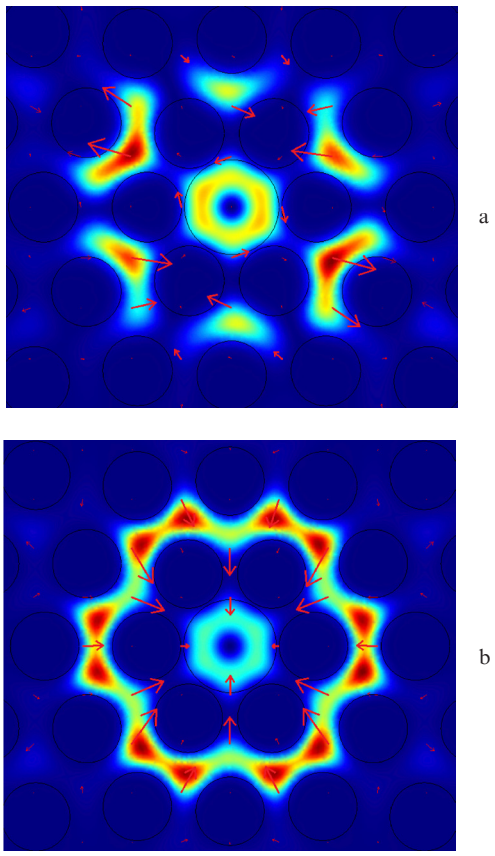

Figure 8. (Colour online) Spatial intensity distributions of (a) mode 4a at a wavelength of 1.640 μm and (b) mode 6a at a wavelength of 1.060 μm.

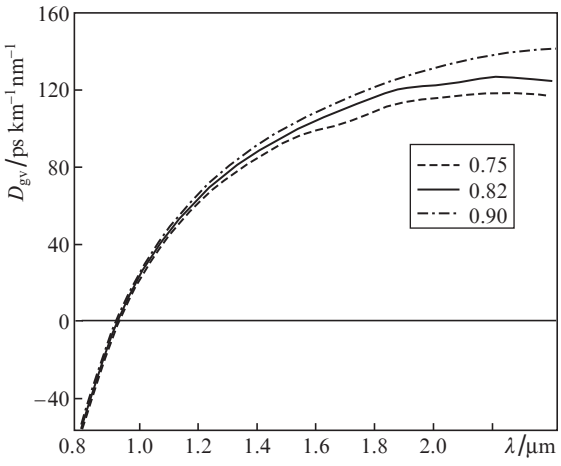

Figure 9. Spectral dependences of group velocity dispersion for the fundamental mode at $d/\Lambda_1 = 0.75$, 0.82, and 0.90.

vice versa. Haakestad and Skaar [18] derived Kramers–Kronig relations for the n_{eff} of modes in optical fibre and showed that, if material dispersion and absorption in a given spectral range can be neglected, the propagation (leakage) loss is an effective component of the losses.

In our case, it is reasonable to believe that changes in leakage loss lead to the corresponding variations in refractive index. Since the spectral dependences of the leakage loss for modes 3a and 3b (Fig. 7a) are opposite in behaviour, the real parts of their effective indices n_{3a} and n_{3b} have opposite devia-

tions from linearity. As a result, we obtain the dependences shown in Figs 7b and 7c. More accurate quantitative calculations are beyond the scope of this work.

There is on the whole a similar picture for the higher order modes 4–6: near each local maximum, we observe pairs of modes – 4a + 4b, 5a + 5b, and 6a + 6b – similar in the spatial intensity distribution in the MOF-30 core. At the same time, there are principal distinctions between the spatial intensity distributions of these modes in the annular space: they are characterized by an inherent azimuthal character different from the distributions of modes 3a and 3b. As an illustration, Fig. 8 shows spatial intensity distributions of modes 4a and 6a at wavelengths of 1.640 and 1.060 μm, respectively. The spectral dependences of the leakage loss, effective indices, and effective index differences for modes 4–6 near their local maxima are qualitatively similar to those for mode 3 (Fig. 7), with slight differences in variations of the corresponding parameters.

Group velocity dispersion D_{gv}, one of the key parameters for supercontinuum generation, is given by [15]

$$D_{gv} \approx -\frac{\lambda}{c}\frac{d^2 n}{d\lambda^2}. \quad (5)$$

Figure 9 shows spectral dependences of D_{gv} for the fundamental mode 1 of MOF-30 at $d/\Lambda_1 = 0.75$, 0.82, and 0.90. From these data, we can determine the corresponding zero-dispersion wavelengths, which differ very little: 932, 927, and 923 nm, respectively. Thus, variations in d/Λ_1 have no significant effect on the zero-dispersion wavelength of MOF-30, and some differences in D_{gv} in the long-wavelength region are not very essential for supercontinuum generation. Such parameters allow MOF-30 to be used for supercontinuum generation with the use of a pulsed laser emitting near 1.06 μm.

The fabrication of the proposed MOF-30 presents no difficulties. To this end, one can drill holes in monolithic silica glass with diamond core drills and then draw the resultant preform into fibre [19]. Unlike a standard process of stacking capillaries and rods, this approach allows for any arrangement of air holes in the preform and, hence, in MOF-30. In the case of identical circular holes, the fabrication of such preforms and MOF-30 drawing from them present no serious problems.

Nevertheless, it is reasonable to further optimize the structure of MOF-30 in order to find configurations with a wider single-mode range. For example, the narrow minimum corresponding to the short-wavelength edge of the single-mode range at $\lambda_{SW} = 0.77$ μm for $d/\Lambda_1 = 0.82$ can be juxtaposed with the broad minimum at $\lambda_{SW} = 1.01$ μm for $d/\Lambda_1 = 0.85$ (Fig. 5a), which may eventually allow an edge at $\lambda_{SW} < 0.77$ μm to be obtained. To this end, a calculation cycle should be performed at constant $d/\Lambda_1 = 0.85$. The width of the annular space should be taken in some range near $Z_{12} = 1.11$ μm (corresponding to $d/\Lambda_1 = 0.82$), and the d/Λ_3 ratio should be varied so as to obtain a fundamental mode leakage loss of 0.1 dB m^{-1} at a wavelength of 2.3 μm.

An important point in the fabrication of MOF-30 is the sensitivity of its parameters, including the short-wavelength edge of its single-mode range, λ_{SW}, to process-related deviations of the parameters of the final product from calculated ones. As seen in Fig. 4, the positions of the local leakage loss maxima for higher order modes are rather sensitive to even slight changes in the width of the annular space, Z_{12}. Because of this, if MOF-30 has a small scatter in the hole size or the spacing between the holes, significant changes in the position, height, and width of the local maxima can be expected. On the other hand, as pointed out above in discussing Fig. 3, these local maxima have a high 'background' level, so on the whole they have essentially no effect on the short-wavelength edge of the single-mode range, λ_{SM}. Therefore, it is reasonable to expect that slight process-related deviations from intended parameters in the fabrication of MOF-30 will not cause marked changes in the single-mode range.

5. Conclusions

A new design of microstructured optical fibres has been proposed. Its characteristic features are that there are three rings of identical circular holes around a circular core, with different separations between the rings, and that the third (outermost) ring is incomplete and consists of only 12 holes, so that the total number of holes in the MOFs is 30. The properties of the fibres have been analysed numerically using the finite element method.

We have obtained spectral dependences of the leakage loss for the fundamental and higher order modes in the range 0.40–2.65 μm at various parameters of the MOFs and demonstrated the presence of local maxima in the spectral dependences of the leakage loss for higher order modes in certain ranges of MOF parameters, which are due to the existence of two modes near each maximum identical in the spatial intensity distribution in the MOF core but differing in additional intensity maxima in the annular space between the first and second rings of holes. Since the modes in each pair have different spectral dependences of the leakage loss, the resultant minimum in the combination of the two spectral dependences has a shape characteristic of a resonance peak. The physical mechanism responsible for the presence of the maxima and the variation of their position with MOF parameters is related to the quasi-resonant effect of MOF-30 structure parameters – primarily of the width of the annular space – on the relationship between the integrated mode intensities in the MOF core and annular space upon variations in wavelength.

It has been shown that the proposed MOF design allows for single-mode operation in the range 0.77–2.3 μm, and approaches for extending the single-mode range of the MOF have been examined. The proposed MOF design can be used e. g. for supercontinuum generation with good beam quality in a wide spectral range.

References

1. Nielsen F.D., Pedersen M.Ø., Qian Y., Andersen T.V., Leick L., Hansen K.P., Pedersen C.F., Thomsen C.L. *Proc. CLEO/Europe and IQEC 2007* (New York: Opt. Soc. Am., 2007) CJ5_4.
2. Xiong C., Wadsworth W.J. *Opt. Express*, **16**, 2438 (2008).
3. Choi H.-G., Kee C.-S., Sung J.H., Yu T.J., Ko D.-K., Lee J., Park H.Y., Kim J.-E. *Phys. Rev. A*, **77**, 035804 (2008).
4. Klarskov P., Isomäki A., Hansen K.P., Andersen P.E. *Opt. Express*, **19**, 26672 (2011).
5. Birks T.A., Knight J.C., Russell P.St.J. *Opt. Lett.*, **22**, 961 (1997).
6. Mortensen N.A., Folkenberg J.R., Nielsen M.D., Hansen K.P. *Opt. Lett.*, **28**, 1879 (2003).
7. White T.P., McPhedran R.C., de Sterke C.M., Botten L.C., Steel M.J. *Opt. Lett.*, **26**, 1660 (2001).
8. Wong W.S., Peng X., McLaughlin J.M., Dong L. *Opt. Lett.*, **30**, 2855 (2005).
9. Fini J.M. *Opt. Express*, **13**, 3477 (2005).
10. Tsuchida Y., Saitoh K., Koshiba M. *Opt. Express*, **15**, 1794 (2007).
11. Dong L., Peng X., Li J. *J. Opt. Soc. Am. B*, **24**, 1689 (2007).

12. Rosa L., Saitoh K., Tsuchida Y., Varshney S.K., Koshiba M., Poli F., Passaro D., Cucinotta A., Selleri S., Vincetti L., in *Integrated Photonics and Nanophotonics Research and Applications* (Optical Society of America, 2008) paper IWB3; https://doi.org/10.1364/IPNRA.2008.IWB3.
13. Saitoh K., Varshney S., Sasaki K., Rosa L., Pal M., Paul M.C., Ghosh D., Bhadra S.K., Koshiba M. *J. Lightwave Technol.*, **29**, 2609 (2011).
14. Saitoh K., Koshiba M. *IEEE J. Quantum Electron.*, **38**, 927 (2002).
15. Agrawal G.P. *Nonlinear Fiber Optics* (San Diego: Academic, 1995; Moscow: Mir, 1996) p. 15.
16. Kuhlmey B.T., McPhedran R.C., de Sterke C.M. *Opt. Lett.*, **27**, 1684 (2002).
17. Guobin R., Zhi W., Shuqin L., Shuisheng J. *Opt. Express*, **11**, 1310 (2003).
18. Haakestad M.W., Skaar J. *Opt. Express*, **13**, 9922 (2005).
19. Denisov A.N., Semjonov S.L., Astapovich M.S., Senatorov A.K. *J. Lightwave Technol.*, **33**, 5184 (2015).